Human Molecular Genetics, 2010, Vol. 19, No. 6 **973–986**
doi:10.1093/hmg/ddp562
Advance Access published on December 18, 2009

Ciliary neurotrophic factor-induced sprouting preserves motor function in a mouse model of mild spinal muscular atrophy

Christian M. Simon[1], Sibylle Jablonka[1], Rocio Ruiz[2], Lucia Tabares[2] and Michael Sendtner[1,*]

[1]Institute for Clinical Neurobiology, Josef-Schneider-Str. 11, 97080 Wuerzburg, Germany and [2]Department of Medical Physiology and Biophysics, School of Medicine, University of Seville, 41009 Seville, Spain

Received August 28, 2009; Revised November 7, 2009; Accepted December 15, 2009

Proximal spinal muscular atrophy (SMA) is caused by homozygous loss or mutation of the *SMN1* gene on human chromosome 5. Depending on the levels of SMN protein produced from a second *SMN* gene (*SMN2*), different forms of the disease are distinguished. In patients with milder forms of the disease, type III or type IV SMA that normally reach adulthood, enlargement of motor units is regularly observed. However, the underlying mechanisms are not understood. *Smn*$^{+/-}$ mice, a mouse model of type III/IV SMA, reveal progressive loss of motor neurons and denervation of motor endplates starting at 4 weeks of age. Loss of spinal motor neurons between 1 month and 12 months reaches 40%, whereas muscle strength is not reduced. In these animals, amplitude of single motor unit action potentials in the gastrocnemic muscle is increased more than 2-fold. Confocal analysis reveals pronounced sprouting of innervating motor axons. As ciliary neurotrophic factor (CNTF) is highly expressed in Schwann cells, we investigated its role for a compensatory sprouting response and maintenance of muscle strength in this mouse model. Genetic ablation of CNTF results in reduced sprouting and decline of muscle strength in *Smn*$^{+/-}$ mice. These findings indicate that CNTF is necessary for a sprouting response and thus enhances the size of motor units in skeletal muscles of *Smn*$^{+/-}$ mice. This compensatory mechanism could guide the way to new therapies for this motor neuron disease.

INTRODUCTION

Spinal muscular atrophy (SMA) is an autosomal recessive disorder with various phenotypes, ranging from severe forms that lead to rapid paralysis and early death in type I patients to milder forms (type III and type IV) in which patients reach normal age despite impairment by muscle paralysis (1,2). A common feature of these various forms is the loss of α-motor neurons in the spinal cord, which causes muscle weakness and muscle atrophy, in particular, in the proximal muscle groups of the body axis (3). All these disease forms are caused by homozygous deficiency and/or mutation of the survival motor neuron gene (*SMN1*) on human chromosome 5, which encodes for the ubiquitously expressed SMN protein (4). It plays a role in the assembly of small nuclear ribonucleoprotein particles (U snRNPs) (5–8), the central components of the spliceosomes. Furthermore, the SMN protein has an additional function, particularly in motor neurons, in promoting presynaptic differentiation by contributing to the translocation of the β-actin mRNA to the presynaptic compartment (9). Thus, Smn-deficiency leads to highly reduced β-actin protein levels and defective clustering of voltage-gated Ca^{2+} channels in axonal growth cones in motor neurons isolated from a mouse model of SMA type I (10). Defects in presynaptic components of neuromuscular junctions and corresponding defects in neuromuscular transmission are also observed in early postnatal mice with this disease (11). This report demonstrated that the loss of synaptic vesicles occurred from active zones in a mouse model of type II SMA, and that the depletion of synaptic vesicles correlated with increased phosphorylated neurofilament in this mouse model. Dysorganized cytoskeletal elements such as increased levels of neurofilament in axon terminals are prominent in mouse models of SMA (12). Recent reports confirm these findings and provide evidence that the accumulation of neurofilaments occurs as part of a dying back process in mouse models of SMA (13).

*To whom correspondence should be addressed. Tel: +49 93120144000; Fax: +49 93120144009; Email: sendtner_m@klinik.uni-wuerzburg.de

In humans, SMA type I becomes clinically apparent within 6 months after birth, SMA type III in the second or third year after birth (14). Disease progression differs between type I and type III SMA. Type I patients die within few years after birth, type III patients normally reach adult age. In some of these patients, disease progression slows down with age, and compensatory mechanisms are thought to underlie this phenomenon (3,14). Mice with inactivation of one allele of *Smn* that show a 50% reduction of SMN protein levels exhibit progressive postnatal loss of spinal motor neurons of up to 50% at an age of 12 months (15), although these mice remain phenotypically unaffected. This indicates that motor function does not correlate with the loss of spinal motor neurons, and that compensatory mechanisms are active in milder forms of SMA but not in the severe forms that lead to early postnatal death.

In order to identify the underlying compensatory mechanisms, we analysed $Smn^{+/-}$ mice electrophysiologically and histopathologically to characterize single motor units. Along with a reduction of motor neurons by over 40%, the size of the average single motor unit action potential (SMUAP) in the gastrocnemic muscle was increased by a factor of at least 2. To investigate how this electrophysiological observation corresponds to changes at the structural level, we analysed axon terminals in the gastrocnemic muscles. We found increased sprouting, a compensatory way to restore nerve–muscle connectivity. CNTF is highly expressed in Schwann cells close to neuromuscular endplates. In order to characterize the role of this neurotrophic factor in this context, $Smn^{+/-}$ mice were crossbred with $Cntf^{-/-}$ mice, and the resulting double mutants investigated by electrophysiology, immunohistochemistry and analysis of muscle strength. In agreement with previous data showing that CNTF can induce terminal sprouting and sprouting from nodes of Ranvier within denervated muscle (16,17), our data suggest that CNTF is necessary for the intramuscular sprouting observed in $Smn^{+/-}$ mice, and thus prevents a drop of muscle strength. This explains why disease progression is slow in type III SMA mouse models in comparison to type I SMA in which sprouting and enlargement of motor units does not normally occur. This finding could guide the way to new therapies in SMA.

RESULTS

Increased mean motor unit size in the gastrocnemic muscle of $Smn^{+/-}$ mice

$Smn^{+/-}$ mice do not develop signs of muscle weakness despite the loss of at least 40% of spinal motor neurons (L1–L7) at an age of 12 months (Fig. 1A and B) (15). To get an insight into the underlying compensatory mechanisms, we analysed motor function of the gastrocnemic muscle by electromyographic (EMG) measurements (18) in 12-month-old $Smn^{+/-}$ and $Smn^{+/+}$ littermate controls. We have chosen the gastrocnemic muscle because it contains large motor units and is more affected than i.e. the small finger muscles in SMA type III patients. Moreover, the innervation pattern of this muscle has been studied in detail (19), and this muscle is easily accessible for electrophysiological analysis and analyses of alterations of motor units such as sprouting (16). We first stimulated the sciatic nerve by a single current pulse of supramaximal amplitude and recorded the maximum compound motor action potential (CMAP), which directly relates to the total number and size of muscle fibres. Despite the loss of lumbar motor neurons in $Smn^{+/-}$ mice at this age (15), the mean amplitude of the maximum CMAP in the $Smn^{+/-}$ mice was not different (data not shown). This finding corresponds to the lack of weakness and normal gross morphology of the gastrocnemic muscle (Fig. 1B and Supplementary Material, Fig. S1) in 12-month-old $Smn^{+/-}$ mice.

We then investigated the size of the motor units by applying successive incremental stimuli (Fig. 1C–E), starting from a subthreshold level, until recruiting 12 individual responses. As shown in Fig. 1C and D, the size of the amplitude increments was larger in $Smn^{+/-}$ than in $Smn^{+/+}$ control mice. The average amplitude of the responses, measured as the mean single motor unit action potential (SMUAP), was more than three times higher in $Smn^{+/-}$ mice than in controls (Fig. 1E), indicating that this massive enlargement of the mean motor unit size is responsible for maintenance of muscle strength in $Smn^{+/-}$ mice. This indicates that compensatory mechanisms allow muscle fibres to remain active in this mouse model of SMA type III despite the loss of motor neurons in the spinal cord (15).

Enhanced arborization of nerve endings in gastrocnemic muscle in 12-month-old $Smn^{+/-}$ mice

Twelve-month-old $Smn^{+/-}$ mice exhibit a reduction in lumbar spinal motor neurons and simultaneously increased amplitudes of SMUAPs in the gastrocnemic muscle. In order to study the underlying structural alterations in motor axons innervating the skeletal muscle and in neuromuscular junctions, we crossed $Smn^{+/-}$ mice with mice expressing the YFP protein under the Thy1 promoter (line YFP-H) in individual motor neurons (20). In these mice, less than 10% of motor neurons express the fluorescent tracer. This allows tracking all terminals of individual motor neurons within the gastrocnemic muscle. We isolated muscles from $Smn^{+/-}$ *thy1-YFP-H*^{tg} and $Smn^{+/+}$ *thy1-YFP-H*^{tg} mice. After counterstaining with Alexa594-conjugated α-bungarotoxin, nerve fibres were visualized in whole mount gastrocnemic muscles by confocal microscopy. The gastrocnemic muscle is innervated by at least three major branches from the tibial nerve (19). We quantified the number of branching points of individual axons in the upper medial branch of the tibial nerve (white arrow in Fig. 2A), because it could be reproducibly identified and analysed in the isolated gastrocnemic muscles. This branch comes from the main trunk and enters the medial gastrocnemic muscle (Fig. 2B). We traced individual axons back from neuromuscular endplates to the trunk of the nerve and counted the number of branching points. Quantification is shown in Fig. 2C. In $Smn^{+/-}$ gastrocnemic muscle, enhanced branching and sprouting of nerve terminals became detectable (Fig. 2C and D). The number of axons with 4, 5 and 6 branches is increased in *Smn* heterozygous deficient mice, and the number of axons with one to three branches is decreased, indicating that enhanced axonal sprouting of terminal motor fibres could be responsible for re-innervation of denervated muscle fibres, due to the loss of spinal motor neurons in the corresponding region of the lumbar spinal cord.

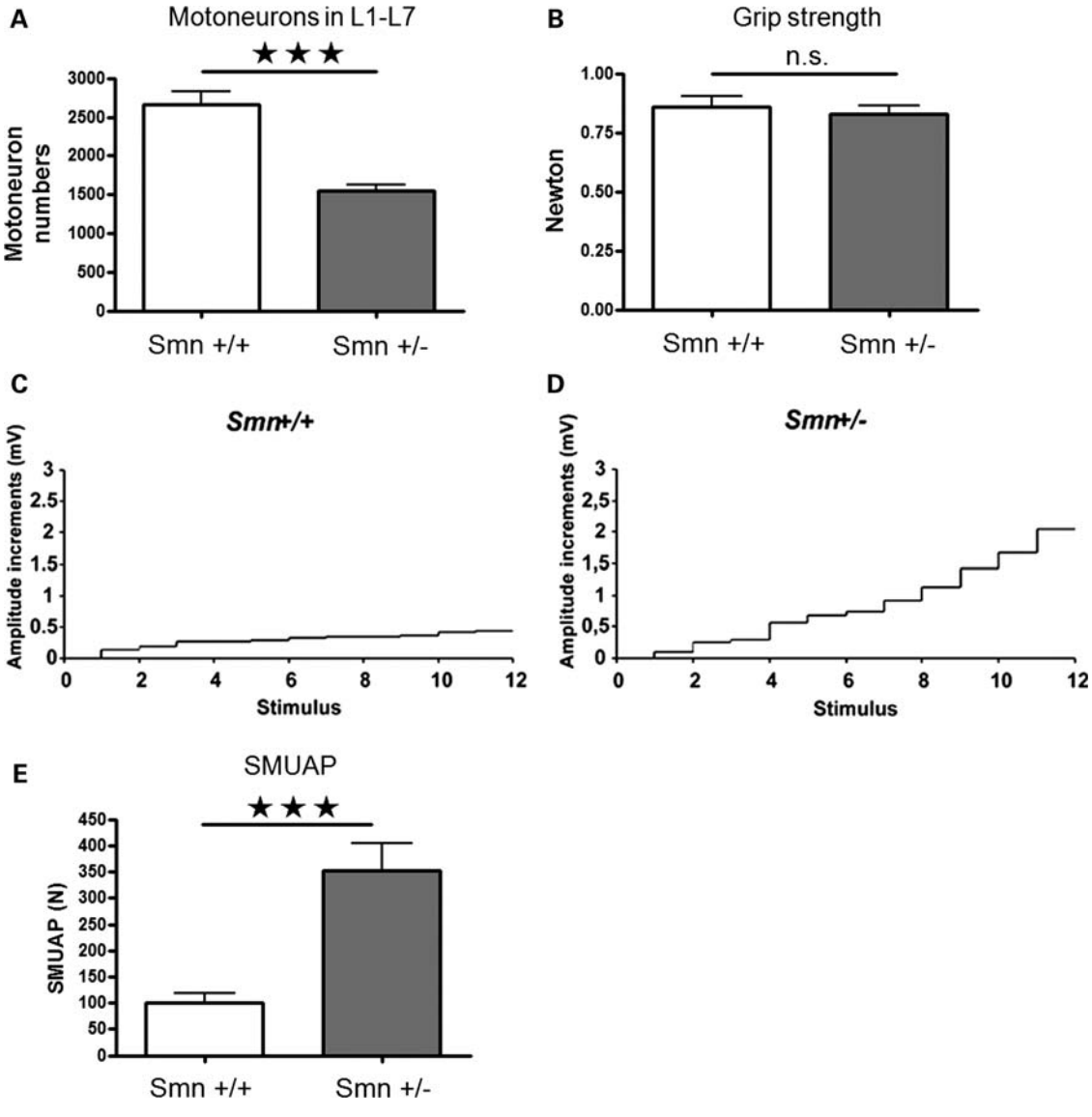

Figure 1. Characterization of motor neuron numbers in lumbar spinal cord and motor unit size in the gastrocnemic muscle of $Smn^{+/-}$ mice. (**A**) Counts of motor neuron cell bodies in the lumbar spinal cord (L1–L7) of 12-month-old $Smn^{+/+}$ ($n = 4$) and $Smn^{+/-}$ ($n = 5$) mice. (**B**) Grip strength in 12-month-old $Smn^{+/+}$ ($n = 5$) and $Smn^{+/-}$ ($n = 8$) mice. (**C** and **D**) Representative examples of SMUAP amplitude increments in gastrocnemic muscle of 1-year-old control (C) and in $Smn^{+/-}$ heterozygous mice (D) in response to 12 nerve stimuli of increasing amplitude after stimulation and recording with needle electrodes. (**E**) Normalized Mean ± SEM SMUAP in WT and $Smn^{+/-}$ mice ($n = 7$). $^{*}P < 0.05$, $^{**}P < 0.01$, $^{***}P < 0.001$.

Development of motor neuron loss, denervation of neuromuscular endplates and compensation by sprouting in $Smn^{+/-}$ mice

In order to find out when denervation and re-innervation of individual neuromuscular endplates first occurs in $Smn^{+/-}$ mice, we counted motor neuron numbers in the lumbar spinal cord (L1–L7) in 4-week and 6-month-old $Smn^{+/-}$ and control mice (Fig. 3). In 4-week-old mice, motor neuron numbers were not reduced (Fig. 3A), whereas 23% loss of motor neurons was observed in 6 month and 42% in 12-month-old $Smn^{+/-}$ mice, thus confirming previously published data (15). This corresponded to enhanced fibre grouping in 12-month-old $Smn^{+/-}$ mice (Supplementary Material, Fig. S2), as visualized by ATPase staining of frozen gastrocnemic muscle sections at pH 4.3 that marks slow twitch fibres. However, despite the loss of motor neurons, no loss of muscle strength was observed in 4-week-, 6-month- and 12-month-old mice (Fig. 3B). First signs of denervation of neuromuscular endplates were already observed in 4-week-old $Smn^{+/-}$ mice (Fig. 3C and D). In 4-week-old gastrocnemic muscles, individual neuromuscular endplates became detectable in which the postsynaptic staining with fluorescence-coupled BTX was not covered by immunofluorescence against neurofilament light chain (NFL), a presynaptic marker of innervating motor axons (Fig. 3D). NFL antibodies were applied in this experiment in order to avoid potential bias caused by the selective expression of YFP. In contrast to NFL antibodies that label all neuromuscular endplates,

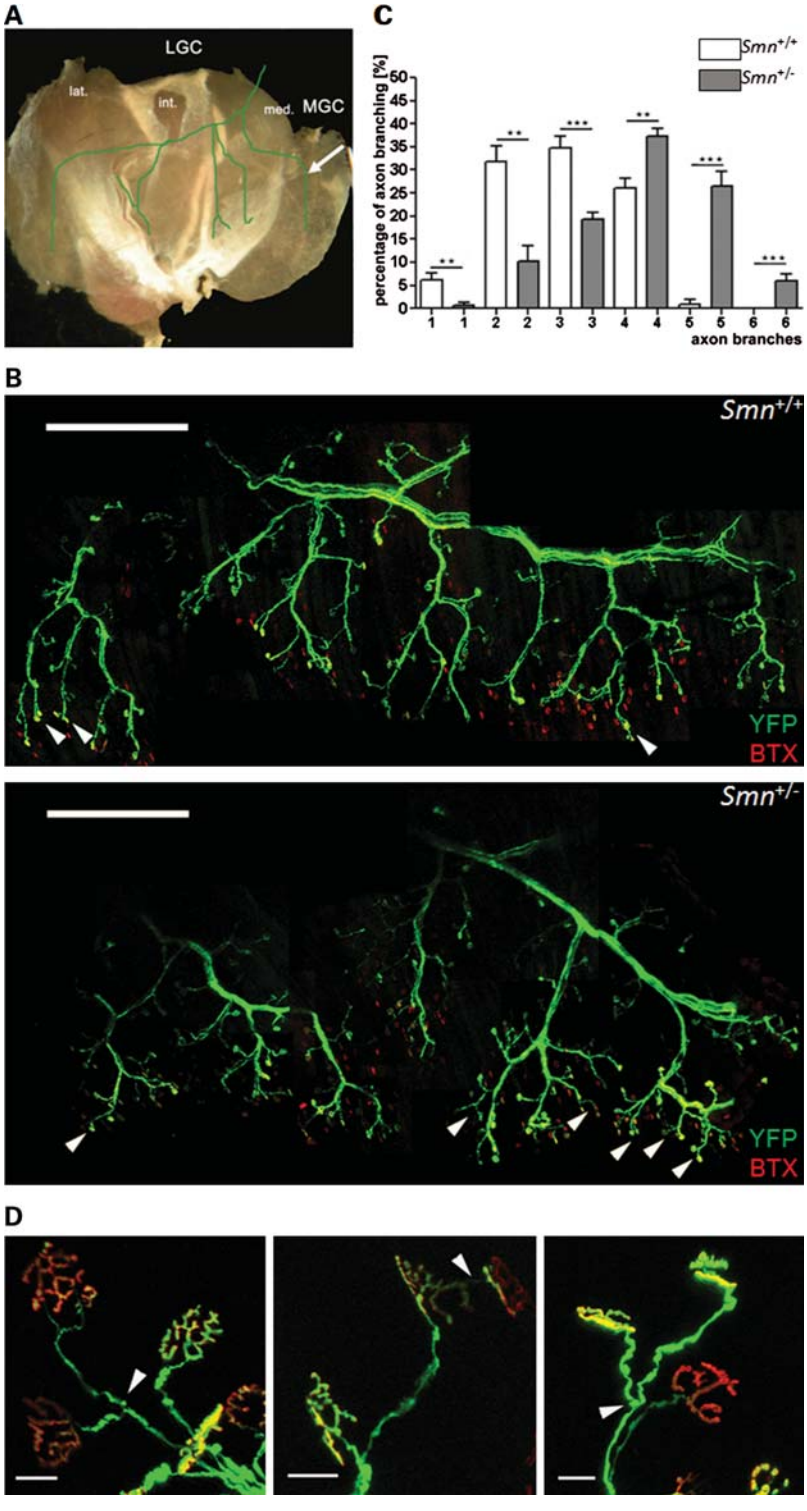

Figure 2. Enhanced arborization and terminal sprouting of motor fibres innervating the gastrocnemic muscle in $Smn^{+/-}$ mice. (**A**) Overview of a mechanically squeezed gastrocnemic muscle and the arborization pattern of the innervating tibial nerve in the muscle whole mount preparation. The arrow points to the investigated area. (**B**) The upper medial branch of the tibial nerve in $Smn^{+/+}$ *thy*1-*YFP-H*^{tg} and $Smn^{+/-}$ *thy*1-*YFP-H*^{tg} mice. Scale bar = 250 μm, arrowheads point to sprouting events. (**C**) Quantification of the arborization level (white bars represent data from $Smn^{+/+}$ *thy*1-*YFP-H*^{tg} mice and grey bars from $Smn^{+/-}$ *thy1-YFP-H*^{tg} mice). Individual axon terminals (at least $n = 50$) were traced back to the main medial branch innervating the MGC muscle as outlined in (A), and the number of branching points were counted. Levels of axon arborization reflect formation of additional branches distal of the main trunk. In $Smn^{+/-}$ gastrocnemic muscle, axons with additional branching points, in particular in the distal segments, are significantly more abundant than in $Smn^{+/+}$ muscle, indicative of enhanced axonal sprouting. In addition, in $Smn^{+/-}$ gastrocnemic muscle, more axons are present that show additional sprouts close to neuromuscular endplates (arrowheads) ($n = 3$ independent animals for each group, muscles from both sides were investigated from each animal). $^{*}P < 0.05$, $^{**}P < 0.01$, $^{***}P < 0.001$. (**D**) High power micrographs of sprouting axons. Arrowheads point to sprouting. The panel in the middle shows terminal sprouting. Scale bar = 20 μm.

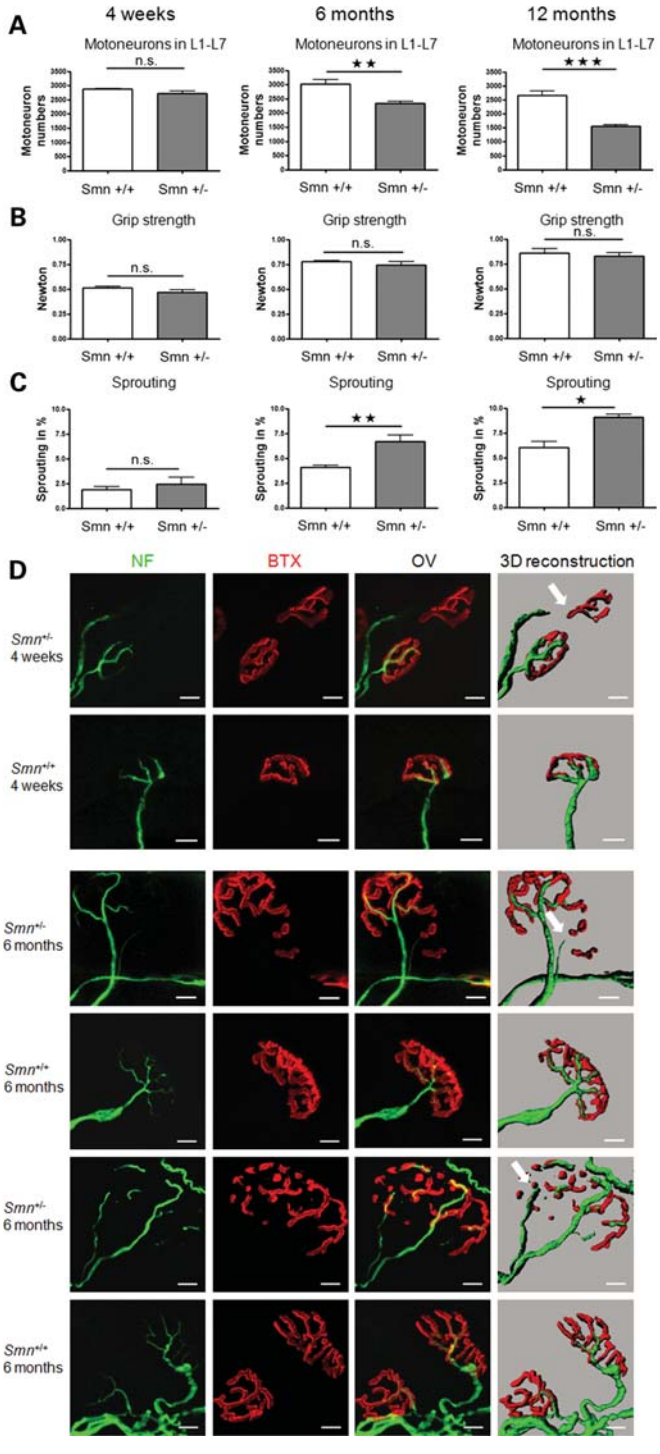

Figure 3. Development of motor neuron loss, denervation and re-innervation of neuromuscular endplates in *Smn*+/− mice. (**A**) Motor neurons were counted in the lumbar spinal cord (L1–L7) of 4-week-, 6-month- and 12-month-old $Smn^{+/-}$ and $Smn^{+/+}$ mice (n = at least 3 for each group). Whereas motor neuron numbers appeared unaffected in 4-week-old $Smn^{+/-}$ mice, a significant loss was observed in 6- and 12-month-old $Smn^{+/-}$ mice. (**B**) Grip strength was unaffected in $Smn^{+/-}$ mice at any stage between 4 weeks and 12 months, indicating that the loss of motor neurons was functionally compensated in $Smn^{+/-}$ mice. (**C**) A significant increase in the frequency of axon terminals innervating two neuromuscular endplates was observed in 6- and 12-month-old $Smn^{+/-}$ mice. A first tendency of enhanced sprouting, although not significant, was also observed in 4-week-old $Smn^{+/-}$ mice. At least 150 axon terminals were investigated per animal in the gastrocnemic muscles from both sides (n = at least three animals per group). (**D**) The figure shows examples of denervated neuromuscular endplates in 4-week-old (upper two panels) and 6-month-old (lower four panels) $Smn^{+/-}$ mice. Morphology of neuromuscular endplates in corresponding control animals ($Smn^{+/+}$ mice from the same litters) is also shown. Denervation is shown by lack of covering of the postsynaptic side of neuromuscular endplates, stained with BTX by innervating axonal branches that are stained with antibodies against neurofilament light chain. The corresponding 3D reconstructions generated from the original confocal stacks with Imaris software are shown on the right side. Individual denervated neuromuscular endplates are marked by arrows. Scale bar = 10 μm. $^{*}P < 0.05$, $^{**}P < 0.01$, $^{***}P < 0.001$.

YFP is expressed in less than 10% of the motor neurons in Thy1-YFP-H mice, a subgroup that is potentially not representative of all lumbar motor neurons. We counted denervated neuromuscular junctions and found 8 from 334 (2.4%, in comparison to 1.7% (6/344) in $Smn^{+/+}$ mice) in the gastrocnemic muscle of 4-week-old $Smn^{+/-}$ animals. At least three independent animals were investigated, with at least 80 neuromuscular junctions screened per animal. Denervation of neuromuscular endplates was more prominent (15/293 corresponding to 5.1%) in 6-month-old $Smn^{+/-}$ mice (Fig. 3D), in comparison to 7/280 (2.5%) in age-matched $Smn^{+/+}$ mice.

For analysis of sprouting, more than 150 endplates in different areas of the gastrocnemic muscle were investigated in order to quantify synapses innervated by axon terminals that had developed terminal branches by sprouting, thus innervating two or more nearby endplates (see also Fig. 5D and E). Compensatory mechanisms by enhanced terminal arborization and sprouting already occurred in 4-week-old $Smn^{+/-}$ mice. In 4-week-old $Smn^{+/-}$ mice, a tendency towards enhanced sprouting was observed (Fig. 3C), and the difference became significant in 6-month-old $Smn^{+/-}$ mice. This confirms previously published data that the disease process in mouse models for SMA reflects a dying back process (13). Our data indicate that denervation of neuromuscular endplates occurs early starting in 4-week-old $Smn^{+/-}$ mice before the loss of motor neuron cell bodies becomes apparent in the lumbar spinal cord. No loss of muscle strength was observed in 4-week-, 6-month- or 12-month-old mice, indicating that the mechanism of compensation for denervation of individual neuromuscular endplates and motor neuron loss are robust in these mice.

Ciliary neurotrophic factor is located in Schwann cells of innervating motor axons in $Smn^{+/-}$ gastrocnemic muscle

In adult mammals, myelinating Schwann cells express high levels of the neurotrophic factor ciliary neurotrophic factor (CNTF). CNTF has also been shown to protect axonal destruction in *pmn* mice, a mouse model for amyotrophic lateral sclerosis (ALS) (21–23). Furthermore, CNTF application protects maintenance of innervation of motor endplates in SOD G93A mice, a mouse model of familial ALS (19). Therefore, we tested expression of CNTF in Schwann cells surrounding motor axons in the gastrocnemic muscle of $Smn^{+/-}$ mice. CNTF immunoreactivity is prominent both in myelinating Schwann cells and in Schwann cells close to neuromuscular junctions (Fig. 4A and B). The specificity of this staining was tested by the analysis of neuromuscular endplates from $Smn^{+/-}$ $Cntf^{-/-}$ and $Smn^{+/+}$ $Cntf^{-/-}$ mice from the same litters (Fig. 4A, third and fourth panel from top). These nerve fibres did not show any CNTF immunoreactivity in surrounding Schwann cells. CNTF expression was also detected in the cytoplasm of myelinating Schwann cells in the sciatic nerve of $Smn^{+/-}$ mice (Fig. 4C), as previously observed in other models of motor neuron diseases such as *pmn* (24) and SOD1 G93A mutant mice (25).

Reduced axonal sprouting in $Smn^{+/-}$ $Cntf^{-/-}$ skeletal muscle

To investigate whether the loss of CNTF reduces compensatory sprouting that is detectable in $Smn^{+/-}$ muscle by morphological and electrophysiological techniques (Figs 1E and 2C), we crossbred $Smn^{+/-}$ with $Cntf^{-/-}$ mice in order to obtain $Smn^{+/-}$ $Cntf^{-/-}$ and corresponding $Smn^{+/-}$ and $Cntf^{+/+}$ control mice. First, we counted numbers of motor neuron cell bodies in the spinal cord (L1–L7). Previous studies (26–28) have shown that $Cntf^{-/-}$ mice exhibit loss of motor neurons between 4 weeks and 6 months. Similar losses of motor neurons were observed in the $Cntf^{-/-}$ mice used in this study (Fig. 5A). Four-week-old mice of all genotypes do not show motor neuron loss (Fig. 5A, Supplementary Material, Fig. S3), and the grip strength was normal in all four genotypes (Fig. 5B). A tendency of enhanced sprouting in $Smn^{+/-}$ was detectable (Fig. 5C).

$Smn^{+/-}$, $Smn^{+/-}$ $Cntf^{+/+}$ and $Smn^{+/-}$ $Cntf^{-/-}$ show a significant loss of motor neurons at 6 and 12 months in comparison to controls (Fig. 5A and Supplementary Material, Fig. S4). However, there were no additive effects of CNTF and Smn deficiency. The difference between $Smn^{+/-}$ $Cntf^{+/+}$ and $Smn^{+/-}$ $Cntf^{-/-}$ was not significant at any age studied. Functional analysis by grip strength measurements (28) revealed a reduction in muscle strength of ~15% in $Cntf^{-/-}$ and $Smn^{+/-}$ $Cntf^{-/-}$ mice. However, although $Smn^{+/-}$ $Cntf^{+/+}$ mice exhibit even higher losses of spinal motor neurons than $Cntf^{-/-}$ mice, there was no reduction in muscle strength at 6 and 12 months. In contrast, 6- and 12-month-old $Smn^{+/-}$ mice that were CNTF-deficient showed reduced muscle strength (Fig. 5B). To address the question whether CNTF-induced sprouting provides a functional compensation for motor neuron losses in $Smn^{+/-}$ $Cntf^{+/+}$ mice, we investigated the innervation pattern of endplates in the gastrocnemic muscle. Therefore, terminal axons were stained with antibodies against neurofilament. More than 150 endplates in different areas of the gastrocnemic muscle were investigated in order to quantify synapses innervated by axon terminals that had developed terminal branches by sprouting, thus innervating two or more nearby endplates. Figure 5D shows a typical innervation pattern found in wild-type control muscles. Some synaptic areas are magnified. In the upper panel (Fig. 5D, 1–4), examples of axons are shown that innervate only one endplate (no sprouting). Figure 5D (5–7) and E shows examples of axons innervating at least two endplates (sprouting). Applying these criteria, we investigated endplates with the nearby axon innervating more than one synapse in $Smn^{+/+}$, $Smn^{+/-}$ $Cntf^{+/+}$, $Cntf^{-/-}$ and $Smn^{+/-}$ $Cntf^{-/-}$. In 6- and 12-month-old $Smn^{+/-}$ $Cntf^{+/+}$ gastrocnemic muscles, the number of axon terminals innervating two endplates (Fig. 5C) is significantly enhanced by a factor of about 2 (Fig. 5C) compared with control $Smn^{+/+}$ mice. In CNTF-deficient mice, only few terminal sprouts were observed, both in $Cntf^{-/-}$ and $Smn^{+/-}$ $Cntf^{-/-}$ mice. These data indicate that CNTF induces sprouting and compensates for the loss of muscle strength in $Smn^{+/-}$ $Cntf^{+/+}$ mice.

Reduction of the mean single motor unit action potential size in $Smn^{+/-}$ $Cntf^{-/-}$ muscle to wild-type levels correlates with reduced muscle strength

To investigate the functional consequences of reduced sprouting after deletion of the *Cntf* gene in $Smn^{+/-}$ mice, we measured muscle strength (Fig. 5B) and the soma size of lumbal motor

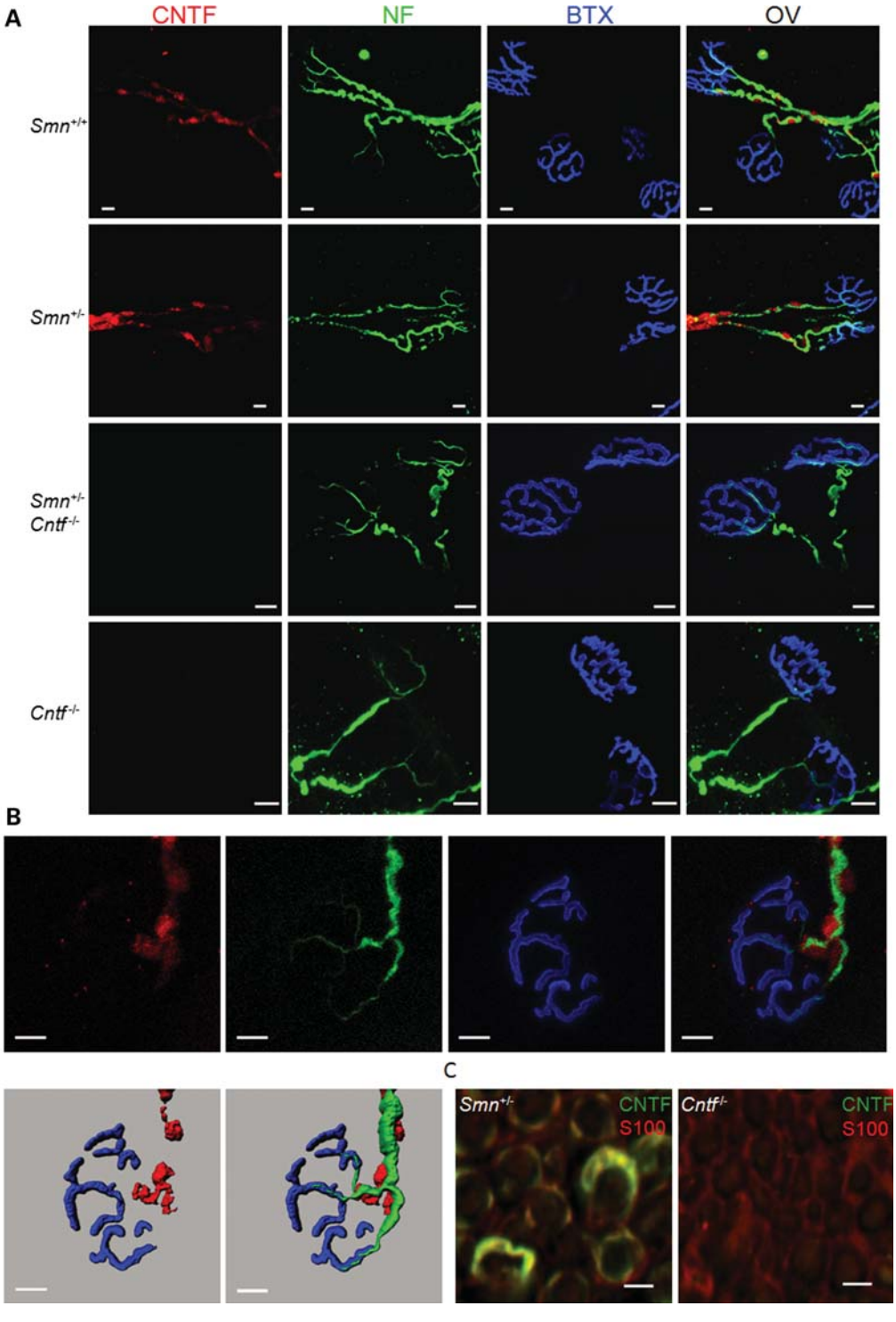

Figure 4. Localization of CNTF immunoreactivity in control and $Smn^{+/-}$ muscle and nerves. (**A**) Localization of CNTF in 100 μm thick longitudinal frozen sections of the gastrocnemic muscle from $Smn^{+/+}$, $Smn^{+/-}$, $Smn^{+/-}$ $Cntf^{-/-}$ double mutant and $Cntf^{-/-}$ mice. Triple staining against α-bungarotoxin (BTX, blue), neurofilament (NF, green) and CNTF (CNTF, red) was performed. Individual channels for CNTF, NF and BTX staining are shown, as well as an overlay (OV) on the right side. In $Smn^{+/+}$ and $Smn^{+/-}$ muscle, CNTF is located in Schwann cells surrounding the axons. As a control, the CNTF signal was undetectable in $Smn^{+/-}$ $Cntf^{-/-}$ double mutant and $Cntf^{-/-}$ single mutant muscle tissues. Scale bar = 10 μm. (**B**) High magnification of a $Smn^{+/-}$ neuromuscular endplate to demonstrate CNTF expression in Schwann cells. Scale bar = 10 μm. A 3D reconstruction of the triple staining, generated by Imaris software from the complete confocal stack, is shown in the lower panel. CNTF immunoreactivity is detectable at high levels around the axons before they enter and branch into the pretzel like structure of the neuromuscular endplate. (**C**) Double staining for CNTF and S100 in frozen sections of the sciatic nerve from $Smn^{+/-}$ and $Cntf^{-/-}$ mice. A S100 antibody was used as a Schwann cell marker in combination with the CNTF antibodies to confirm the localization of CNTF in the Schwann cells, as seen in Fig. 3A. CNTF colocalizes with S100 in the cytoplasm of Schwann cells and in $Smn^{+/-}$ nerves. No signal for CNTF was detected in $Cntf^{-/-}$ nerve. Scale bar = 5 μm.

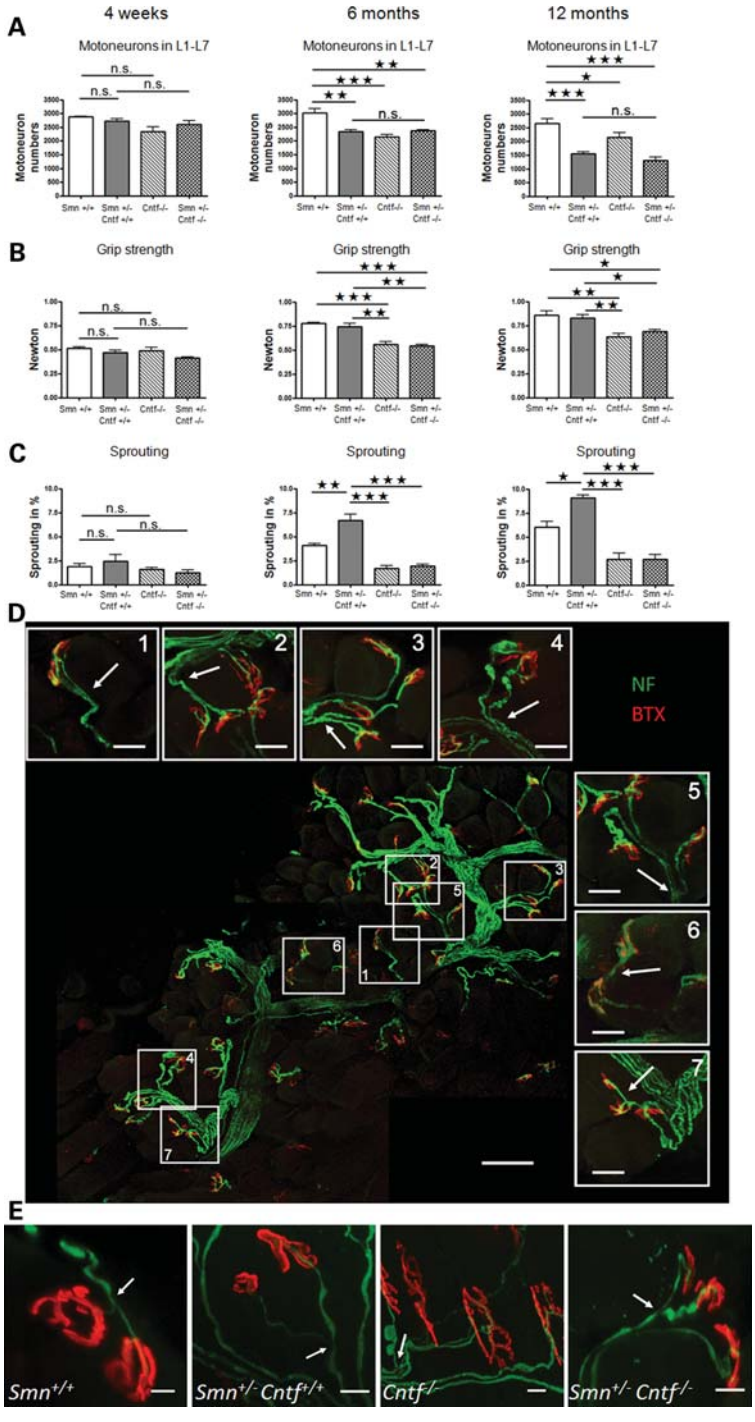

Figure 5. Lack of CNTF abolishes the sprouting of motor nerves in the gastrocnemic muscle of $Smn^{+/-}$ mice. (**A**) Counts of motor neuron cell bodies in the lumbar spinal cord (L1–L7) of 4-week-, 6-month- and 12-month-old $Smn^{+/+}$ ($n = 3$), $Smn^{+/-}$ $Cntf^{+/+}$ ($n = 5$), $Cntf^{-/-}$ ($n = 3$) and $Smn^{+/-}$ $Cntf^{-/-}$ double mutant mice ($n = 4$). (**B**) Grip strength in 4-week- ($n =$ at least 3 in each group), 6-month- ($n =$ at least 3 in each group) and 12-month-old $Smn^{+/+}$ ($n = 5$), $Smn^{+/-}$ $Cntf^{+/+}$ ($n = 8$), $Cntf^{-/-}$ ($n = 5$) and $Smn^{+/-}$ $Cntf^{-/-}$ ($n = 5$) mice. (**C**) Quantification of axonal sprouting, using the same technique as in Fig. 2C. In $Smn^{+/-}$ $Cntf^{+/+}$ muscles, a significantly increased number of synapses innervated by collateral or terminal sprouts was observed in comparison to $Smn^{+/+}$ muscle at 6 and 12 months. Increased sprouting in $Smn^{+/-}$ $Cntf^{+/+}$ mice was abolished when CNTF was depleted in $Smn^{+/-}$ $Cntf^{-/-}$ double deficient mice. At least 150 neuromuscular endplates were investigated per animal ($n =$ at least 3 in each group). (**D**) Overview of the innervation pattern in the gastrocnemic muscle of a 12-month-old wild-type mouse stained with α-bungarotoxin and antibodies against neurofilament in order to trace all motor axons. Seven areas with neuromuscular synapses were magnified to demonstrate terminal sprouting. The upper panel shows examples of neuromuscular endplates with axon terminals innervating only one endplate (no sprouting, indicated by arrows). The right column shows rare examples of axon terminals innervating more than one endplate (sprouting, indicated by arrows). Scale bar overview = 100 μm, scale bar magnified area = 30 μm. In total, more than 150 endplates were investigated for each genotype to quantify the frequency of terminal sprouting. (**E**) Examples of neuromuscular endplates in gastrocnemic muscle from mice with the four different genotypes. Arrows point to the position of terminal sprouts. Scale bar = 10 μm. $^{*}P < 0.05$, $^{**}P < 0.01$, $^{***}P < 0.001$.

neurons of the spinal cord (L4–L5) of 4-week and 12-month-old mice (Supplementary Material, Fig. S5). We found a slightly increased number of motor neurons with a size over 1000 μm^2 in 12-month-old $Smn^{+/-}$ $Cntf^{+/+}$ mice. We also performed electrophysiological analyses to determine the size of individual motor units. Using a ring electrode placed at mid-thigh, the mean single motor unit action potential (SMUAPs) sizes in $Smn^{+/+}$, $Smn^{+/-}$ $Cntf^{+/+}$, $Cntf^{-/-}$ and $Smn^{+/-}$ $Cntf^{-/-}$ were estimated by applying successive incremental stimuli starting from a subthreshold level until recruiting 10 individual responses (Fig. 6A). As shown before by the results obtained with the needle electrode placed into the gastrocnemic muscle (Fig. 1C-E), $Smn^{+/-}$ $Cntf^{+/+}$ mice show about two times larger SMUAPs than $Smn^{+/+}$ mice. $Cntf^{-/-}$ mice exhibit lower SMUAPs than $Smn^{+/-}$ mice. $Smn^{+/-}$ $Cntf^{-/-}$ exhibit almost 4-fold lower SMUAPs than $Smn^{+/-}$ mice (Fig. 6B). This result indicates that motor units are smaller in the double mutant mouse. These data confirm the functional relevance of the morphological alterations shown in Figure 5. In Figure 6C, a summary of the progressive loss of motor neurons in $Smn^{+/-}$ $Cntf^{+/+}$ mice from 4 weeks to 12 months is shown. In 6-month-old mice, the loss is ~20%, and reaches over 40% in 12-month-old-mice. To maintain the same grip strength, axonal sprouting and size of motor units increase correspondingly. Thus, CNTF appears necessary for the compensatory sprouting response that maintains muscle strength in $Smn^{+/-}$ $Cntf^{+/+}$ mice.

DISCUSSION

$Smn^{+/-}$ mice, a mouse model of mild forms of SMA, can maintain muscle strength by compensatory increase of the amplitude of single motor action potentials in skeletal muscle. The loss of motor neurons is thus compensated by sprouting from remaining motor axon terminals so that neuromuscular endplates remain innervated. Lack of CNTF that is highly expressed in Schwann cells surrounding axon terminals reduces this sprouting response, both on a morphological and functional level as determined by electrophysiological analyses and by measurement of muscle strength.

The most severe form of spinal muscular atrophy, SMA type I or Werdnig–Hoffmann disease, differs from the milder forms SMA type II, type III and type IV by its fast progression and the high mortality in early childhood (3,14). Similarly, $Smn^{-/-}$ $SMN2^{tg}$ mice that express two copies of the human *SMN2* gene on a mouse *Smn* null background, die within few days after birth, and these mice do not survive beyond postnatal day 6 (29). However, this mouse model of type I SMA shows only relatively moderate motor neuron loss in the spinal cord (17%) (29) at a final stage of the disease when the mice are completely paralytic at 3–5 days after birth. The fast progression of the disease points to an absence of compensatory mechanisms in comparison to mouse models with a more moderate phenotype and a slower disease progression, as it has been found in $Smn^{+/-}$ mice, a model for SMA type III (15). This corresponds to observations that survival of isolated $Smn^{-/-}$ $SMN2^{tg}$ motor neurons in cell culture is not impaired, but that axon growth (9) and presynaptic differentiation are disturbed. Defective axon growth and dysfunction of neuromuscular transmission have also been observed in Smn-deficient zebrafish (30), fly larvae (31) and mice (11,32,33). In contrast, $Smn^{+/-}$ mice that lack only 50% of Smn protein levels survive and do not show any overt sign of motor neuron disease despite a progressive and significant loss of motor neuron cell bodies. These motor neurons are apparently able to sprout and to re-innervate motor endplates that would become denervated when motor neurons are lost. This correlates with an increase in the amplitude of motor units. Similar electrophysiological findings, the lack of abnormal spontaneous activity and large motor units have also been made in patients with milder forms of SMA (3). Our data indicate that CNTF is responsible for the sprouting response that leads to this enlargement of motor units and thus compensates for loss of motor neurons in the milder forms of the disease.

Why does CNTF not compensate in the severe forms of SMA in $Smn^{-/-}$ $SMN2^{tg}$ mice? CNTF expression is low during embryonic development (34,35), and in the peripheral nervous system CNTF expression only becomes upregulated in Schwann cells starting at the end of the first postnatal week (34,36). In rodents, CNTF expression reaches the high levels found in the adult nervous system in the third postnatal week. Therefore, CNTF is not present during the first days after birth when these mice become severely paralyzed (29) and show pathology such as depletion of synaptic vesicles at active zones and reduced synaptic transmission (11).

Addition of CNTF by application via CNTF-secreting stem cells (21) or by local injection into skeletal muscle (23) leads to improved maintenance of motor axons in peripheral nerves of *pmn* mutant mice or neuromuscular endplates in SOD G93A mice (19). Interestingly, this effect appears relatively specific for CNTF, as other neurotrophic factors for motor neurons such as the glial-derived neurotrophic factor (GDNF) were without any effect in the same disease models (19,23).

Schwann cells close to neuromuscular endplates play a major role in triggering terminal sprouting (37,38). As shown here, these cells express CNTF, and lack of CNTF expression strongly reduces terminal sprouting and augmentation of motor unit size. Terminal Schwann cells have been found to express Semaphorin-3, and it has been suggested that the upregulation of Semaphorin-3 in terminal Schwann cells could suppress sprouting and contribute to loss of neuromuscular synapses in motor neuron disease (39). Other studies have shown that the depletion of synaptic vesicles precedes the loss of synapses in a mouse model of ALS, and that CNTF could prevent the depletion of synaptic vesicles and thus maintain function of these synapses. This effect of CNTF correlates with reduced accumulation of neurofilaments (19), a characteristic hallmark of motor neuron disease in Smn deficient mice (11–13) and in SOD G93A mice, and reduced expression of stress-related genes such as Bcl-2a1-a that are normally upregulated in SOD G93A mice at a stage when synapse loss occurs. How could CNTF act on maintenance of motor endplates and induction of sprouting in $Smn^{+/-}$ mice? After binding to the CNTF receptor complex, classical signalling pathways are activated, including B-Raf (40) and the phosphatidylinositol 3 kinase (PI-3K) pathways, that do not only maintain survival but also mediate effects on the cytoskeleton (41). In addition, activation of the CNTF receptor

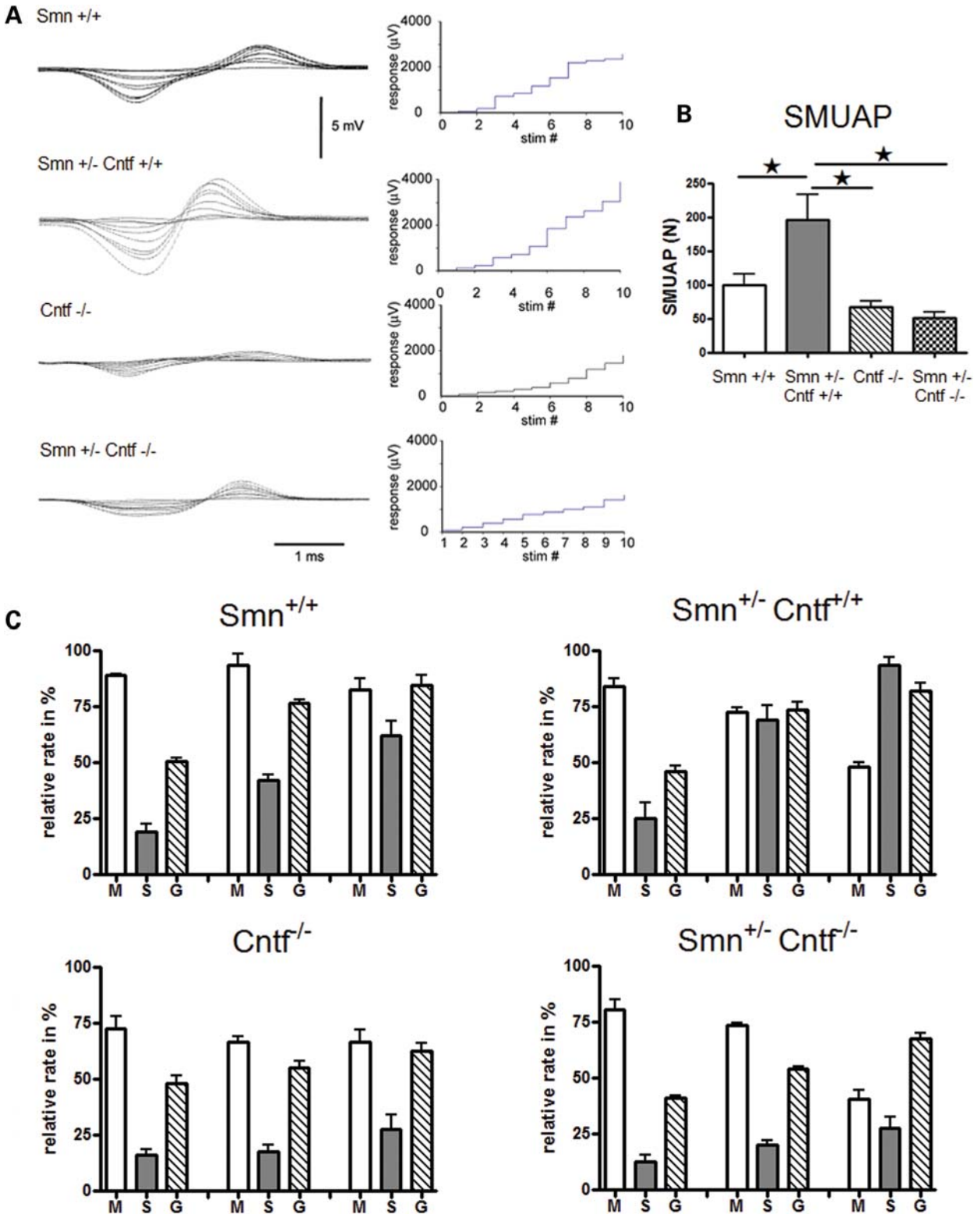

Figure 6. Lack of CNTF abolishes the compensatory increase of motor unit size in *Smn*$^{+/-}$ mice. (**A**) Representative examples of SMUAP amplitude increments recorded from 1-year-old *Smn*$^{+/+}$, *Smn*$^{+/-}$ *Cntf*$^{+/+}$, *Cntf* $^{-/-}$ and *Smn*$^{+/-}$ *Cntf* $^{-/-}$ mice in response to 10 nerve stimuli of increasing amplitude. A circumferential surface electrode was placed around the flexor and extensor compartments of the distal hind-limb. (**B**) Quantification of normalized SMUAP (mean ± SEM) in *Smn*$^{+/+}$ ($n = 15$), *Smn*$^{+/-}$ *Cntf*$^{+/+}$ ($n = 17$), *Cntf* $^{-/-}$ ($n = 9$) and *Smn*$^{+/-}$ *Cntf* $^{-/-}$ ($n = 7$) mice. The amplitude of SMUAPs was increased in *Smn*$^{+/-}$ mice, pointing to increased size of motor units due to increased sprouting. In *Smn*$^{+/-}$ *Cntf*$^{-/-}$ mice, SMUAP amplitudes were not increased. (**C**) Summary of motor neuron numbers, (M), grip strength (G) and number of axons innervating at least two neighbouring neuromuscular endplates (S) in 4-week-, 6-month- and 12-month-old mice of all four genotypes. Values are given as percentage relative to the highest value in each investigation.

complex leads to activation of Stat-3. Interestingly, activated Stat-3 that is phosphorylated at Ser 727 has been shown to affect mitochondrial potential in non-neuronal cells, and it is tempting to speculate that a local effect of activated Stat-3 on mitochondria (42) is responsible for the effects of CNTF on synapse maintenance and sprouting. This finding is in agreement with the observation that in a mouse model with conditional inactivation of the *Stat3* gene in motor neurons, these cells are more vulnerable in adult stages after nerve lesion (43).

Why is the progression of the disease in CNTF-deficient $Smn^{+/-}$ mice not accelerated? CNTF is a member of a large family of neurotrophic cytokines that bind to receptor complexes involving gp130 and LIF-Rβ receptor subunits as signal transducing subunits. This family includes leukaemia inhibitory factor (LIF), which is also expressed in Schwann cells, and cardiotrophin-1. Analysis of double and triple mutant mice for these factors has shown that atrophy of neuromuscular endplates and loss of muscle strength increases if more than one of these ligands is missing (28). When LIF-Rβ is ablated, these mice die at birth because they are unable to breathe and feed (44). Despite these severe signs of paralysis, they exhibit only a loss of 40% of motor neurons, indicating that the loss of neuromuscular transmission rather than the loss of motor neuron cell bodies is responsible for the severe phenotype. Taken together, these data suggest that CNTF is not the only ligand for maintenance of neuromuscular endplates in this mouse model, but it plays a predominant role for the induction of sprouting in this mouse model for mild forms of SMA.

Unfortunately, when CNTF is given systemically to human patients with motor neuron disease, it elicits severe side-effects such as fever and cachexia (45), most probably due to effects on liver cells (46) and cells of the immune system. These side-effects preclude its use for therapy in SMA patients. Recently, techniques have been developed for local application of growth factors such as VEGF to motor neurons and neuromuscular endplates (47). It is possible that such new strategies for growth factor delivery could reduce side-effects associated with systemic delivery. The local expression of CNTF appears attractive under circumstances when endogenous CNTF expression is low, at developmental stages when myelination of peripheral nerves is still incomplete. In summary, our observation that sprouting in milder forms of SMA prevents the decline of muscle strength despite massive loss of spinal motor neurons could guide the way for development of therapies for severe forms of SMA in which such sprouting reactions do not occur.

MATERIALS AND METHODS

Electrophysiological analysis of the gastrocnemic muscle of $Smn^{+/-}$ mice

Compound muscular action potentials (CMAPs) were recorded as described (48) in anaesthetized mice (tribromethanol 2%, 0.15 ml/10 g body weight, i.p.). Stimulating needle electrodes were placed at the sciatic notch and the head of the fibula. The active recording needle electrode was placed into the medial part of the gastrocnemic muscle, or at mid-thigh when a circumferential surface electrode was used. The reference electrode was inserted at the base of the fifth foot phalanx. A ground electrode was placed at the base of the tail. Supramaximal responses were first recorded, followed by responses to incremental currents, in very small steps, from subthreshold levels until the progressive recruitment of 10–12 responses. Each current amplitude was applied three times, and responses were considered stable and therefore acceptable if they were identical.

Preparation of the gastrocnemic muscle for immunohistochemistry and confocal analysis

The $Smn^{+/-}$ and $Cntf^{+/-}$ mice used in this study had been backcrossed at least five times to C57Bl/6 mice, and subsequently every third generation in order to maintain them on a clean C57Bl/6 background. They were housed in the central animal facilities of the University of Wuerzburg. The animal care and ethic committees of our institutions approved all described procedures and experiments. Mice were killed by cervical dislocation, and the native gastrocnemic muscle was dissected and placed on a cover slip. It was immediately covered with 4% paraformaldehyde (PFA) in phosphate buffered saline (Dulbecco's PBS 1× from PAA) and mechanically squeezed by a second cover slip. After 5 min of squeezing, the flattened gastrocnemic muscle was processed further for immunohistochemistry.

Thy1-YFP-H^{tg} mice whole mount preparation of the gastrocnemic muscle

The gastrocnemic muscles from adult $Smn^{+/+}$ *thy1-YFP-H*^{tg} and $Smn^{+/-}$ *thy*1-*YFP-H*^{tg} mice were fixed with 4% paraformaldehyde (PFA) for 2 h. After fixation of the gastrocnemic muscles, they were washed in 1 × PBS and 0.5% Triton X-100 (Sigma) two times for 30 min. YFP is expressed in less than 10% of the motor neurons and their axonal processes in *thy*1-*YFP-H*^{tg} mice (20). The postsynaptic part of neuromuscular endplates was stained with α-bungarotoxin Alexa Fluor 594 (1:500, Molecular Probes) for 30 min. The tissue was then washed in 1× PBS for 2 h. Finally, the tissue was mounted with a DABCO-solution (9.97% PBS, 89.77% Glycerin and 0.26% DABCO). Pictures were taken with the SP2 confocal microscope from Leica, and an Olympus FluoView™ FV1000 confocal microscope with three channel detectors. For quantification of the enhanced arborization in the upper medial branch of the tibial nerve, we traced individual axons back from neuromuscular endplates to the trunk of the nerve and counted the number of branching points.

Neurofilament staining in the whole mount gastrocnemic muscle

The gastrocnemic muscles of $Smn^{+/+}$, $Smn^{+/-}$, $Cntf^{-/-}$; $Smn^{+/-}$ $Cntf^{-/-}$ were fixed in 4% PFA for 2 h. After washing with 1× PBS and 1% Triton X-100 two times for 30 min, the postsynaptic part of neuromuscular endplates was stained with α-bungarotoxin Alexa Fluor 594 (1:500) in 1× PBS and 1% Triton X-100 for 30 min. Subsequently, the tissue was washed in 1× PBS and 1% Triton X-100 for 2 h,

and a blocking solution containing 3% bovine serum albumin (BSA, Sigma) and 5% Triton X-100 to penetrate into the thick muscles was applied for 4 h. Rabbit anti-neurofilament antibodies (150 kDa AB1981, Chemicon) were diluted 1:350 in the blocking solution and applied over night at 4°C. Thereafter, the muscles were washed three times for 30 min in 1× PBS and 1% Triton X-100. As second antibody, swine anti-rabbit FITC (1:40, Dako) was diluted in the blocking solution and applied for 4 h at room temperature. Finally, the tissue was washed three times in 1× PBS and 1% Triton X-100 for 30 min and mounted with DABCO. The pictures were taken with an Olympus FluoView™ FV1000 microscope. For 3D reconstruction, 2D confocal stacks were saved in an Olympus.oib format and opened in Bitplane Imaris 5.7.0 Software supplied by Olympus. An isosurface was generated with a Gaussian filter width of 0.3 μm.

Preparation and staining of cryostat slices of the gastrocnemic muscle and sciatic nerve

Mice were perfused with 4% PFA and the gastrocnemic muscles and the sciatic nerves were prepared. These tissues were postfixed in 4% PFA for 2 h and then transferred into buffer with increasing (10–30%) sucrose content. After the tissue was submerged in the 30% sucrose solution, it was embedded in Tissue Tek (Sakura) and frozen within 2-methylbutane cooled with liquid N_2. Subsequently, the gastrocnemic muscles were cut in 100 μm thick longitudinal sections and the sciatic nerve in 10 μm thick cross-sections with the cryostat. For immunostaining, the sections were blocked with 5% BSA and 0.5% Triton X-100 in 1× TBS for 1 h. The gastrocnemic muscles were stained with α-bungarotoxin Alexa Fluor 594 (1:500), mouse anti-neurofilament (1:350, SMI31R, Covance.) and rabbit anti-CNTF (K10, 1:1000) (26) diluted in blocking solution, whereas the sciatic nerves were stained with mouse anti-S100 (1:350, beta-subunit, Sigma) and rabbit anti-CNTF. After washing three times per 10 min, Cy5 goat anti-mouse (1:200, Jackson Immuno) and swine anti-rabbit FITC (1:350, Dako) for the muscles and Cy3 goat anti-mouse (1:200, Jackson Immuno) and swine anti-rabbit FITC for the nerves were applied for 2 h. Finally, the tissue was washed three times for 10 min and mounted in DABCO, and investigated with the Olympus FluoView™ FV1000 microscope. For a 3D reconstruction, 2D confocal stacks were saved in an Olympus.oib format and opened in Bitplane Imaris 5.7.0 Software supplied by Olympus. An isosurface was generated with a Gaussian filter width of 0.3 μm.

Grip strength measurements

Grip strength measurement was performed with a Digital Force Gauge DFL 2 from Chatillon with every mouse tested at least 10 times, and the mean was taken (26).

Nissl staining of spinal cord sections, quantification of motor neurons in spinal cord sections

Mice were deeply anaesthetized and transcardially perfused with 4% PFA. 12.5 μm paraffin serial sections of the spinal cord were prepared for Nissl staining, as described previously (28). Cresyl violet stains acidic structures within cells intensively, and thus makes the nucleolus and the rough endoplasmatic reticulum visible. Motor neurons differ by a distinct nucleolus and prominent rough endoplasmatic reticulum from other types of neurons in the spinal cord, in particular the interneurons. Even atrophic motor neurons can be clearly distinguished by this technique, as previously shown in *Cntf/Lif/Ct-1* triple deficient mice (28), *bcl-2* deficient mice (49) and *Smn−/−SMN2tg* mice, a mouse model of type I SMA (29). Only motor neurons with clearly distinguishable nucleolus and Nissl stained rough endoplasmatic reticulum-like structure in the cell body were counted in every 10th section of the lumbar spinal cord (L1–L7). Raw counts were corrected for double counting of split nucleoli as described (26).

Myosin ATPase reaction and muscle fibre typing

The gastrocnemic muscle was freshly prepared from mice after cervical dislocation and frozen immediately in nitrogen-cooled 2-methylbutane. ATPase staining was performed on 10 μm thick cryosections under acidic (pH 4.3 and 4.6) and basic (pH 9.4) conditions. Data presented in this study are from reactions at pH 4.3. Type I (slow twitch) muscle fibres are resistant to acidic conditions and show ATPase activity and therefore stain dark. Type 2 (A and B) fibres are not resistant and do not stain. Type 2C fibres show intermediate (gray colour) staining.

HE staining and quantification of muscle fibre size

The muscle was prepared from mice immediately after cervical dislocation and freshly frozen in nitrogen-cooled 2-methylbutane. Ten μm thick cryosections were prepared and stained with a standard HE protocol. The calibre of 150 muscle fibres per muscle biopsy and animal was analysed.

Statistics

Results are reported as means ± SEM. The student's *t*-test was performed as unpaired, two-tailed sets of array. One-way ANOVA with the Tukey's post-test was used to compare more than two groups. Analysis was made by GraphPad Prizm Software (San Diego). Significance level was set as $P < 0.05$.

SUPPLEMENTARY MATERIAL

Supplementary Material is available at *HMG* online.

ACKNOWLEDGEMENTS

We thank Katrin Walter for excellent technical assistance.

Conflict of Interest statement. None declared.

FUNDING

This work was supported by grants from the Deutsche Forschungsgemeinschaft, SFB581, project B1, and from the Hermann und Lilly Schilling Stiftung im Stifterverband der Deutschen Wissenschaft, and a grant from the Spanish Ministery of Education and Science, BFU2007-61171 and BES2005-6739.

REFERENCES

1. Roberts, D.F., Chavez, J. and Court, S.D. (1970) The genetic component in child mortality. *Arch. Dis. Child*, **45**, 33–38.
2. Munsat, T.L. and Davies, K.E. (1992) International SMA consortium meeting. (26–28 June 1992, Bonn, Germany). *Neuromuscul. Disord.*, **2**, 423–428.
3. Crawford, T.O. and Pardo, C.A. (1996) The neurobiology of childhood spinal muscular atrophy. *Neurobiol. Dis.*, **3**, 97–110.
4. Lefebvre, S., Burglen, L., Reboullet, S., Clermont, O., Burlet, P., Viollet, L., Benichou, B., Cruaud, C., Millasseau, P., Zeviani, M. *et al.* (1995) Identification and characterization of a spinal muscular atrophy-determining gene. *Cell*, **80**, 155–165.
5. Liu, Q. and Dreyfuss, G. (1996) A novel nuclear structure containing the survival of motor neurons protein. *EMBO J.*, **15**, 3555–3565.
6. Meister, G., Eggert, C. and Fischer, U. (2002) SMN-mediated assembly of RNPs: a complex story. *Trends Cell Biol.*, **12**, 472–478.
7. Fischer, U., Liu, Q. and Dreyfuss, G. (1997) The SMN-SIP1 complex has an essential role in spliceosomal snRNP biogenesis. *Cell*, **90**, 1023–1029.
8. Buhler, D., Raker, V., Luhrmann, R. and Fischer, U. (1999) Essential role for the tudor domain of SMN in spliceosomal U snRNP assembly: implications for spinal muscular atrophy. *Hum. Mol. Genet.*, **8**, 2351–2357.
9. Rossoll, W., Jablonka, S., Andreassi, C., Kroning, A.K., Karle, K., Monani, U.R. and Sendtner, M. (2003) Smn, the spinal muscular atrophy-determining gene product, modulates axon growth and localization of beta-actin mRNA in growth cones of motoneurons. *J. Cell Biol.*, **163**, 801–812.
10. Jablonka, S., Beck, M., Lechner, B.D., Mayer, C. and Sendtner, M. (2007) Defective Ca2+ channel clustering in axon terminals disturbs excitability in motoneurons in spinal muscular atrophy. *J. Cell Biol.*, **179**, 139–149.
11. Kong, L., Wang, X., Choe, D.W., Polley, M., Burnett, B.G., Bosch-Marce, M., Griffin, J.W., Rich, M.M. and Sumner, C.J. (2009) Impaired synaptic vesicle release and immaturity of neuromuscular junctions in spinal muscular atrophy mice. *J. Neurosci.*, **29**, 842–851.
12. Cifuentes-Diaz, C., Nicole, S., Velasco, M.E., Borra-Cebrian, C., Panozzo, C., Frugier, T., Millet, G., Roblot, N., Joshi, V. and Melki, J. (2002) Neurofilament accumulation at the motor endplate and lack of axonal sprouting in a spinal muscular atrophy mouse model. *Hum. Mol. Genet.*, **11**, 1439–1447.
13. Murray, L.M., Comley, L.H., Thomson, D., Parkinson, N., Talbot, K. and Gillingwater, T.H. (2008) Selective vulnerability of motor neurons and dissociation of pre- and post-synaptic pathology at the neuromuscular junction in mouse models of spinal muscular atrophy. *Hum. Mol. Genet.*, **17**, 949–962.
14. Dubowitz, V. (1995) *Muscle Disorders*, Saunders, London.
15. Jablonka, S., Schrank, B., Kralewski, M., Rossoll, W. and Sendtner, M. (2000) Reduced survival motor neuron (Smn) gene dose in mice leads to motor neuron degeneration: an animal model for spinal muscular atrophy type III. *Hum. Mol. Genet.*, **9**, 341–346.
16. Gurney, M.E., Yamamoto, H. and Kwon, Y. (1992) Induction of motor neuron sprouting in vivo by ciliary neurotrophic factor and basic fibroblast growth factor. *J. Neurosci.*, **12**, 3241–3247.
17. Siegel, S.G., Patton, B. and English, A.W. (2000) Ciliary neurotrophic factor is required for motoneuron sprouting. *Exp. Neurol.*, **166**, 205–212.
18. McComas, A.J., Sica, R.E., Campbell, M.J. and Upton, A.R. (1971) Functional compensation in partially denervated muscles. *J. Neurol. Neurosurg. Psychiatry*, **34**, 453–460.
19. Pun, S., Santos, A.F., Saxena, S., Xu, L. and Caroni, P. (2006) Selective vulnerability and pruning of phasic motoneuron axons in motoneuron disease alleviated by CNTF. *Nat. Neurosci.*, **9**, 408–419.
20. Feng, G., Mellor, R.H., Bernstein, M., Keller-Peck, C., Nguyen, Q.T., Wallace, M., Nerbonne, J.M., Lichtman, J.W. and Sanes, J.R. (2000) Imaging neuronal subsets in transgenic mice expressing multiple spectral variants of GFP. *Neuron*, **28**, 41–51.
21. Sendtner, M., Schmalbruch, H., Stöckli, K.A., Carroll, P., Kreutzberg, G.W. and Thoenen, H. (1992) Ciliary neurotrophic factor prevents degeneration of motor neurons in mouse mutant progressive motor neuronopathy. *Nature*, **358**, 502–504.
22. Sagot, Y., Tan, S.A., Baetge, E., Schmalbruch, H., Kato, A.C. and Aebischer, P. (1995) Polymer encapsulated cell lines genetically engineered to release ciliary neurotrophic factor can slow down progressive motor neuronopathy in the mouse. *Europ. J. Neurosci.*, **7**, 1313–1322.
23. Sagot, Y., Rosse, T., Vejsada, R., Perrelet, D. and Kato, A.C. (1998) Differential effects of neurotrophic factors on motoneuron retrograde labeling in a murine model of motoneuron disease. *J. Neurosci.*, **18**, 1132–1141.
24. Sendtner, M., Götz, R., Holtmann, B. and Thoenen, H. (1997) Endogenous ciliary neurotrophic factor is a lesion factor for axotomized motoneurons in adult mice. *J. Neurosci.*, **17**, 6999–7006.
25. Giess, R., Holtmann, B., Braga, M., Grimm, T., Muller-Myhsok, B., Toyka, K.V. and Sendtner, M. (2002) Early onset of severe familial amyotrophic lateral sclerosis with a SOD-1 mutation: potential impact of CNTF as a candidate modifier gene. *Am. J. Hum. Genet.*, **70**, 1277–1286.
26. Masu, Y., Wolf, E., Holtmann, B., Sendtner, M., Brem, G. and Thoenen, H. (1993) Disruption of the CNTF gene results in motor neuron degeneration. *Nature*, **365**, 27–32.
27. Sendtner, M., Götz, R., Holtmann, B., Escary, J.-L., Masu, Y., Carroll, P., Wolf, E., Brehm, G., Brulet, P. and Thoenen, H. (1996) Cryptic physiological trophic support of motoneurons by LIF disclosed by double gene targeting of CNTF and LIF. *Current Biol.*, **6**, 686–694.
28. Holtmann, B., Wiese, S., Samsam, M., Grohmann, K., Pennica, D., Martini, R. and Sendtner, M. (2005) Triple knock-out of CNTF, LIF, and CT-1 defines cooperative and distinct roles of these neurotrophic factors for motoneuron maintenance and function. *J. Neurosci.*, **25**, 1778–1787.
29. Monani, U.R., Sendtner, M., Coovert, D.D., Parsons, D.W., Andreassi, C., Le, T.T., Jablonka, S., Schrank, B., Rossol, W., Prior, T.W. *et al.* (2000) The human centromeric survival motor neuron gene (SMN2) rescues embryonic lethality in Smn(−/−) mice and results in a mouse with spinal muscular atrophy. *Hum. Mol. Genet.*, **9**, 333–339.
30. McWhorter, M.L., Monani, U.R., Burghes, A.H. and Beattie, C.E. (2003) Knockdown of the survival motor neuron (Smn) protein in zebrafish causes defects in motor axon outgrowth and pathfinding. *J. Cell Biol.*, **162**, 919–931.
31. Chan, Y.B., Miguel-Aliaga, I., Franks, C., Thomas, N., Trulzsch, B., Sattelle, D.B., Davies, K.E. and van den Heuvel, M. (2003) Neuromuscular defects in a Drosophila survival motor neuron gene mutant. *Hum. Mol. Genet.*, **12**, 1367–1376.
32. McGovern, V.L., Gavrilina, T.O., Beattie, C.E. and Burghes, A.H. (2008) Embryonic motor axon development in the severe SMA mouse. *Hum. Mol. Genet.*, **17**, 2900–2909.
33. Kariya, S., Park, G.H., Maeno-Hikichi, Y., Leykekhman, O., Lutz, C., Arkovitz, M.S., Landmesser, L.T. and Monani, U.R. (2008) Reduced SMN protein impairs maturation of the neuromuscular junctions in mouse models of spinal muscular atrophy. *Hum. Mol. Genet.*, **17**, 2552–2569.
34. Stöckli, K.A., Lottspeich, F., Sendtner, M., Masiakowski, P., Carroll, P., Götz, R., Lindholm, D. and Thoenen, H. (1989) Molecular cloning, expression and regional distribution of rat ciliary neurotrophic factor. *Nature*, **342**, 920–923.
35. Stöckli, K.A., Lillien, L.E., Näher-Noe, M., Breitfeld, G., Hughes, R.A., Thoenen, H. and Sendtner, M. (1991) Regional distribution, developmental changes and cellular localization of CNTF-mRNA and protein in the rat brain. *J. Cell Biol.*, **115**, 447–459.
36. Rende, M., Muir, D., Rouslathi, E., Hagg, T., Varon, S. and Manthorpe, M. (1992) Immunolocalization of ciliary neuronotrophic factor in adult rat sciatic nerve. *Glia*, **5**, 25–32.
37. Son, Y.J. and Thompson, W.J. (1995) Nerve sprouting in muscle is induced and guided by processes extended by Schwann cells. *Neuron*, **14**, 133–141.
38. Son, Y.J., Trachtenberg, J.T. and Thompson, W.J. (1996) Schwann cells induce and guide sprouting and reinnervation of neuromuscular junctions. *Trends Neurosci.*, **19**, 280–285.

39. De Winter, F., Vo, T., Stam, F.J., Wisman, L.A., Bar, P.R., Niclou, S.P., van Muiswinkel, F.L. and Verhaagen, J. (2006) The expression of the chemorepellent Semaphorin 3A is selectively induced in terminal Schwann cells of a subset of neuromuscular synapses that display limited anatomical plasticity and enhanced vulnerability in motor neuron disease. *Mol. Cell Neurosci.*, **32**, 102–117.
40. Wiese, S., Pei, G., Karch, C., Troppmair, J., Holtmann, B., Rapp, U.R. and Sendtner, M. (2001) Specific function of B-Raf in mediating survival of embryonic motoneurons and sensory neurons. *Nat. Neurosci.*, **4**, 137–142.
41. Markus, A., Zhong, J. and Snider, W.D. (2002) Raf and akt mediate distinct aspects of sensory axon growth. *Neuron*, **35**, 65–76.
42. Wegrzyn, J., Potla, R., Chwae, Y.J., Sepuri, N.B., Zhang, Q., Koeck, T., Derecka, M., Szczepanek, K., Szelag, M., Gornicka, A. *et al.* (2009) Function of mitochondrial Stat3 in cellular respiration. *SCI*, **323**, 793–797.
43. Schweizer, U., Gunnersen, J., Karch, C., Wiese, S., Holtmann, B., Takeda, K., Akira, S. and Sendtner, M. (2002) Conditional gene ablation of Stat3 reveals differential signaling requirements for survival of motor neurons during development and after nerve injury in the adult. *J. Cell Biol.*, **156**, 287–297.
44. Li, M., Sendtner, M. and Smith, A. (1995) Essential function of LIF receptor in motor neurons. *Nature*, **378**, 724–727.
45. ALS CNTF Treatment Study (ACTS) group. (1996) A double-blind placebo-controlled clinical trial of subcutaneous recombinant human ciliary neurotrophic factor (rhCNTF) in amyotrophic lateral sclerosis. *Neurology*, **46**, 1244–1249.
46. Dittrich, F., Thoenen, H. and Sendtner, M. (1994) Ciliary neurotrophic factor: pharmakokinetics and acute phase response. *Ann. Neurol.*, **35**, 151–163.
47. Azzouz, M. (2006) Gene therapy for ALS: progress and prospects. *Biochim. Biophys. Acta*, **1762**, 1122–1127.
48. Ruiz, R., Lin, J., Forgie, A., Foletti, D., Shelton, D., Rosenthal, A. and Tabares, L. (2005) Treatment with trkC agonist antibodies delays disease progression in neuromuscular degeneration (nmd) mice. *Hum. Mol. Genet.*, **14**, 1825–1837.
49. Michaelidis, T.M., Sendtner, M., Cooper, J.D., Airaksinen, M., Holtmann, B., Meyer, M. and Thoenen, H. (1996) Inactivation of the bcl-2 gene results in progressive degeneration of motoneurons, sensory and sypathetic neurons during early postnatal development. *Neuron*, **17**, 75–89.